Kovove Mater. 52 2014 377–385
DOI: 10.4149/km_2014_6_377

Stress-strain analysis of plane specimens made from R7T steel

M. Štamborská[1]*, V. Mareš[2], M. Kvíčala[1], L. Horsák[2]

[1] *VŠB – Technical University of Ostrava, Faculty of Metallurgy and Materials Engineering, Department of Non-Ferrous Metals, Refining and Recycling, Ostrava – Poruba, Czech Republic*
[2] *VŠB – Technical University of Ostrava, CPIT – Centre for Advanced Innovation Technology, 17. listopadu 15, Ostrava – Poruba, Czech Republic*

Received 1 July 2014, received in revised form 25 August 2014, accepted 10 September 2014

Abstract

The article is focused on the stress analysis of plane specimens made from hypocutectoid steel, using digital image correlation. It is steel used in the manufacture of railway wheels for freight transport.

The aim of the article is to measure the displacement fields by using digital image correlation, from which the strain fields are subsequently calculated. By processing the obtained values using the virtual fields method, the isotropic elastic constants and the hardening behaviour were obtained, which are used to calculate the subsequent stress fields, and they are also used to draw a diagram of engineering and true stress. The maximum average values of stress obtained from true stress – true strain diagram were 990 ± 21 MPa and from engineering diagram 897 ± 18 MPa. The deviation between maximum true and engineering average values of stress was 9 %. The stress fields obtained for 25 and 58 % strains are illustrated in the article.

K e y w o r d s: digital image correlation, virtual fields method, true stress-true strain diagram, engineering diagram

1. Introduction

R7T material is used in the manufacture of railway wheels for freight transport, but always with a hardened annular section. Verification of the quality through various tests is essential outside monitored dimensional characteristics [1–4]. One of the basic tests is the tensile test, by which we can characterize the plastic properties of materials.

Identification and quantification of the plastic deformation of materials is important for many reasons. Overloading of bearing elements of constructions commonly leads to the plastic deformation of materials and to their damage. The knowledge of the distribution and the size of plastic deformation make better use of the material properties in the manufacture of components and also in their operation [5–8].

Characterization of the material properties can be made by a uniaxial tensile test and by using the virtual fields method (VFM). The advantage of using full measurements in the identification process is that one test can provide more information. Grédiac, Pieron and Avril stated the overview of the virtual fields method (VFM) and its application in the elastic and plastic range [9].

In experimental analysis of plastic deformation on the surface of specimens is advantageous to use contactless displacement sensing methods, allowing to obtain deformation fields in pre-selected areas. The digital image correlation (DIC) is one of the most advanced optical methods of displacement sensing and subsequent determination of strains on the surface of examined objects [10–14].

Due to the fact that it was the analysis of plane task, a single scanning device was used, where the displacement fields were obtained on the specimen surface. The strain fields were calculated from the displacement fields by the Vic 2D program. The Matlab program calculated the stress fields in reaching 25 and 58 % of strains after obtaining the parameters in

*Corresponding author: tel.: +420 597 329 421; e-mail address: stamborska.michaela@gmail.com

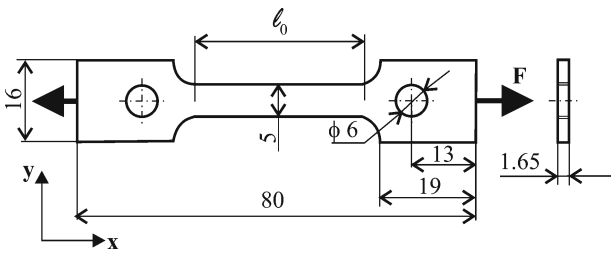

Fig. 1. Geometry of plane specimen (mm).

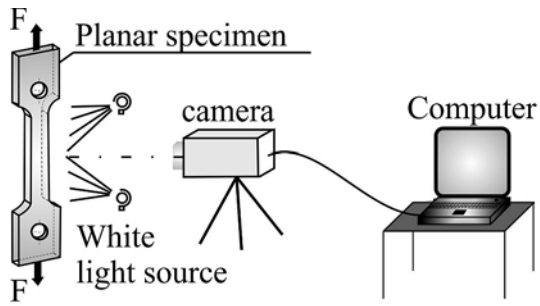

Fig. 2. The method principle of 2D digital image correlation.

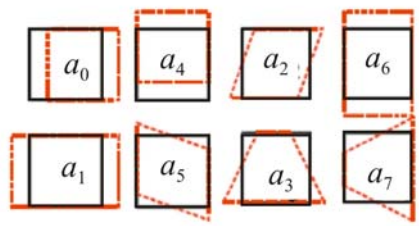

Fig. 3. Transformation parameters of potential translation, stretch, shear and distortion.

elastic and plastic range, and subsequently a diagram of engineering and true stress was drawn.

2. Experiment methodology

The experiment was carried out on three specimens made from R7T steel, their geometry is shown in Fig. 1.

R7T steel is a hypocutectoid steel for the manufacture of railway wheels. It is defined by European standard EN13262. By default, the steel of a railway wheel is heat-treated in the following manner: austenitization was carried out at 850 ℃, followed by cooling in a water bath and subsequent tempering at 520 ℃. The obtained structure is formed by lamellar pearlite and by a small amount of ferrite.

The material taken from the ring parts of the rail wheel was used for testing and specimen production. The test was carried out on the plane specimens clamped into the clamps of the Zwick/Roel Z150 tensile machine, which were loaded steadily by increasing force. Evaluation of the strain fields was carried out by using image correlation software Vic 2D and the Canon 5D Mark II was used for scanning.

The method of digital image correlation (DIC) is one of the non-interferometric contactless methods for determining the deformation on the surface of objects, and therefore it does not require a coherent light source. Deformation of the surface is determined by comparing the dependence (correlation) of changes in the intensity of grey colour in the monitored area of the object surface, before and after the deformation. In principle, the DIC optical measuring method is based on digital image processing and its numerical analysis.

Only one camera is needed to record digital image of the surface before and after deformation for plane (2D) strain analysis. The surface of measured specimen must be plane and at deformation, it must remain in the same plane, perpendicular to the camera. Any displacements of the surface from the scanning plane must be negligibly small compared to the shift of scanning plane, while the geometry of the image sensing arrangement during the measurement must be maintained.

Experimental determination of plastic deformation by the DIC method will be presented by the measurements at the uniaxial load of plane specimens (Fig. 2).

A contrast black and white random pattern has to be created on the object surface to avoid comparison of non-identical parts of the object. This pattern imitates the object contour, deforms and moves with it together. Displacement and strain fields are determined by correlation of corresponding facets before and after deformation. System realizes calculations with the assistance of correlation algorithm based on pseudo-affine coordinate transformation of object points from one picture to the second one. If a_0, a_1, a_2, …, a_7 are the transformation parameters of potential translation, stretch, shear and distortion (Fig. 3), then:

$$x_t(a_0, a_1, a_2, a_3, x, y) = a_0 + a_1 x + a_2 y + a_3 xy, \quad (1)$$

$$y_t(a_4, a_5, a_6, a_7, x, y) = a_4 + a_5 x + a_6 y + a_7 xy. \quad (2)$$

These parameters are determined by minimizing the distance between the observed grey pattern $G_2(x, y)$ in the second image and the original pattern $G_1(x, y)$ and by applying the photogrammetric corrections as follows:

$$\min_{a_0,\ldots,a_7,g_0,g_1} \sum_{x,y} \|G_1(x, y) - G_T(x, y)\|. \quad (3)$$

The term $G_T(x, y)$ represents an intensity change of grey points during loading and can be expressed as:

Table 1. Chemical composition of the R7T steel, detected by an optical emission spectrometry with a glow discharge (wt.%)

C	Mn	Si	P	S	Cr	Ni	Mo	Cu	Ti	Al
0.385	0.824	0.496	0.007	0.003	0.240	0.074	0.010	0.010	0.001	0.022

Table 2. Selected mechanical properties of R7T steel

$R_{p0.2}$ (MPa)	R_m (MPa)	A_{10} (%)	Hardness (HV_{10})	Fracture toughness K_{IC} (MPa $m^{1/2}$)
515	837	14.1	228	87.96

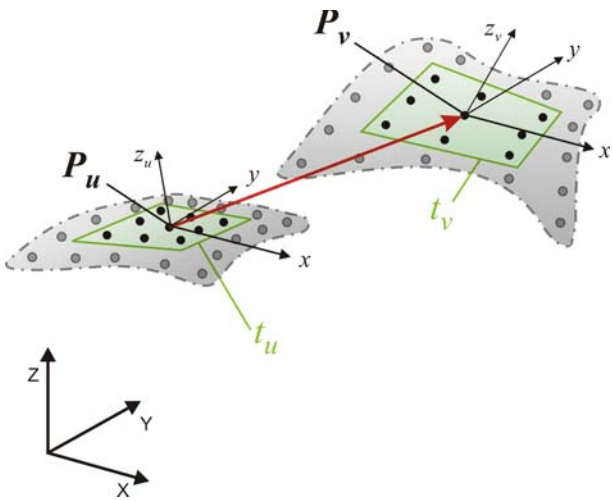

Fig. 4. Determination of the displacement vector.

$$G_T(x,y) = g_0 + g_1 \cdot G_2(x_t(x,y), y_t(x,y)), \qquad (4)$$

where g_0 and g_1 are the illumination parameters.

Figure 4 shows the element displacement vector of the object surface. Centre P was shifted from the reference position u to the deformed position v. In addition, the element surface was rotated, inclined and curved. If displacement vectors of all points and reference outline are known, then it is possible to calculate the strain fields. These can be determined directly by derivative of adjoining points displacements or by analysis of local facets bending, which were used for correlation.

3. Results and discussion

3.1. Material parameters of steel

The chemical composition of steel was detected by an optical emission spectrometry and is shown in Table 1.

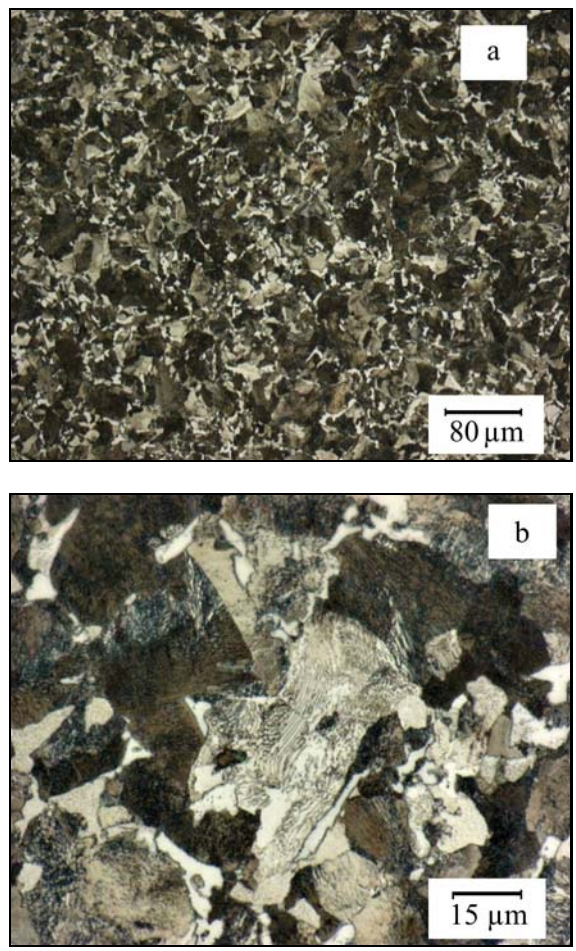

Fig. 5. Microstructure of R7T steel: microstructure at a low magnification (a), detail of the microstructure with the lamellae pearlite (b).

Regarding to the metallographic analysis, the structure of the material was formed by the lamellar pearlite bounded by ferritic cross linking. The structures (Figs. 5, 6) were obtained by standard metallographic procedure, by grinding – polishing – etching in 3 % nital solution, and the photographs were obtained

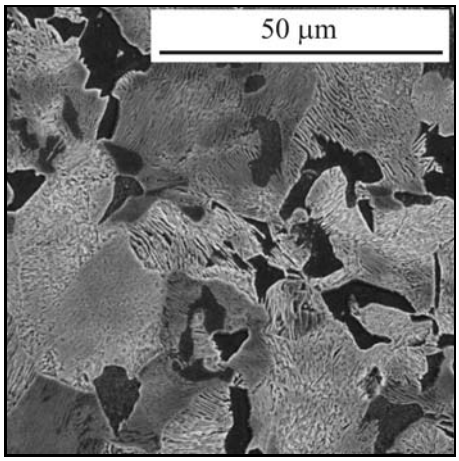

Fig. 6. Microstructure of the R7T steel – pearlite lamellae (electron microscope).

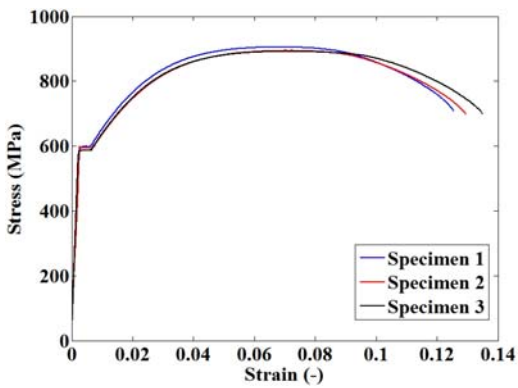

Fig. 7. Contractual stress-strain diagram for all specimens.

by using optical and electron microscope.

Mechanical properties shown in Table 2 were obtained by standard tensile tests of cylindrical specimens and by fracture toughness tests of CT30 bodies.

The stress-strain diagram was obtained by a conventional tensile test on the Zwick/Roel Z150 tensile machine for all three specimens and is shown in Fig. 7.

3.2. Strain fields obtained by Vic 2D software and FEM

Displacements and strain fields of the individual points were determined on the basis of correlation of corresponding facets, before and after deformation. In a case of plane image correlations, the object deformations were determined by an observation through one camera directed perpendicularly to the surface of the object. This procedure was allowed to determine the deformation of the object in a level parallel to the image level of the camera. For visualization, Fig. 8 shows strain fields ε_x, ε_y and γ_{xy} (–) obtained by the Vic 2D software for 25 % strain, when the deformation accu-

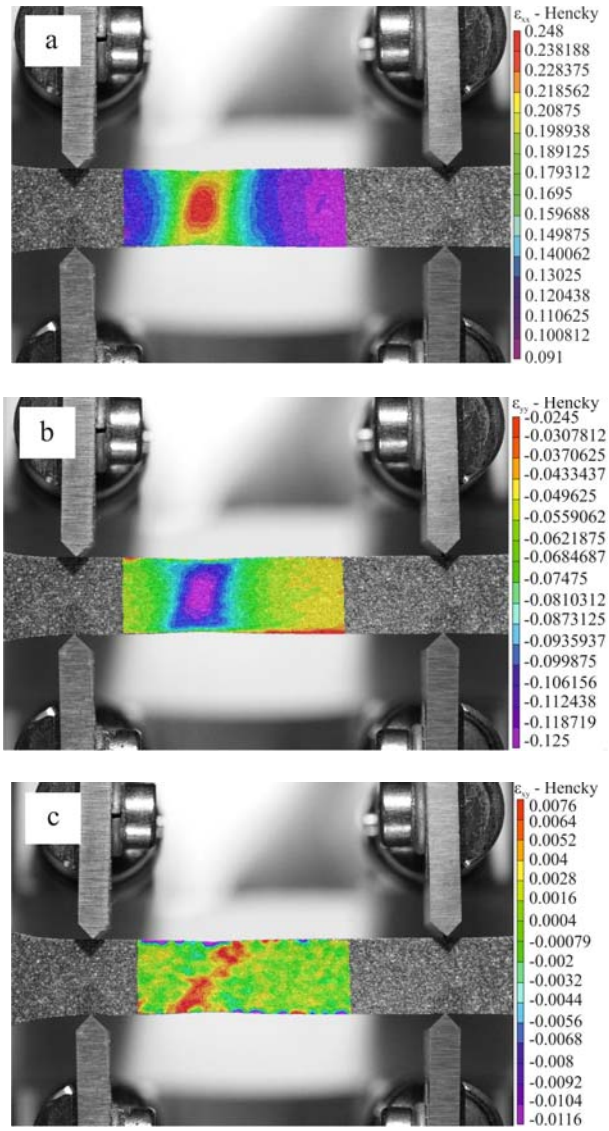

Fig. 8a,b,c. Strain fields ε_x, ε_y and γ_{xy} (–) obtained by the VIC 2D for 25 % strain.

mulated into one place, which preceded creation of the neck. The following results of strains and stresses were measured and calculated for the specimen 1.

FEM model was prepared for comparison of the results obtained by digital image correlation. The results of plastic strain fields ε_x, ε_y and γ_{xy} (–) for comparison with Fig. 8 are shown in Fig. 9.

For visualization, Fig. 10 shows strain fields ε_x, ε_y and γ_{xy} (–) obtained by the Vic 2D software for 58 % strain, where was a significant component distortion with created neck, followed by a disruption of the component.

The results of plastic strain fields ε_x, ε_y and γ_{xy} (–) for comparison with Fig. 10 are shown in Fig. 11.

The strain rate versus time diagram is shown in Fig. 12.

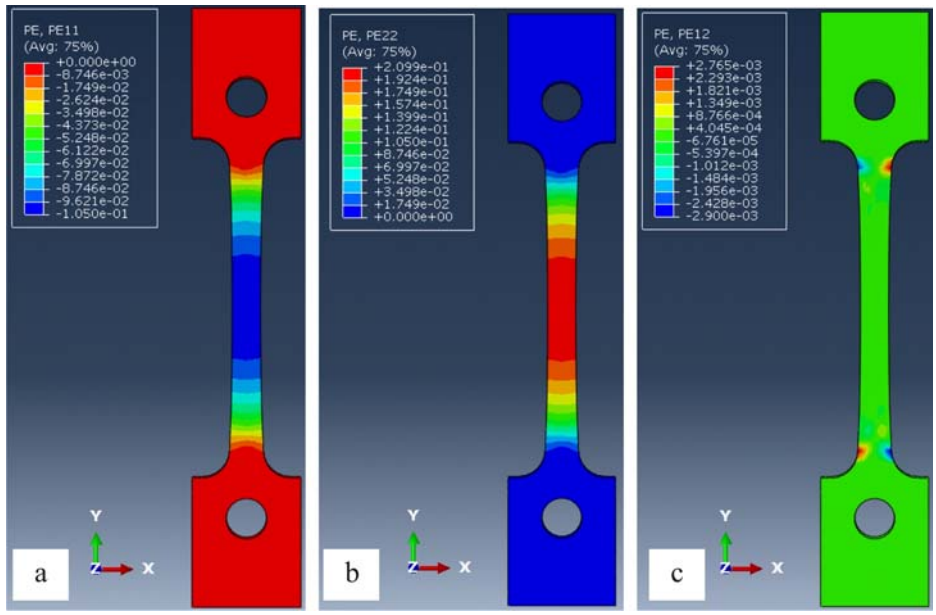

Fig. 9a,b,c. Plastic strain fields ε_x, ε_y and γ_{xy} (–) obtained by FEM.

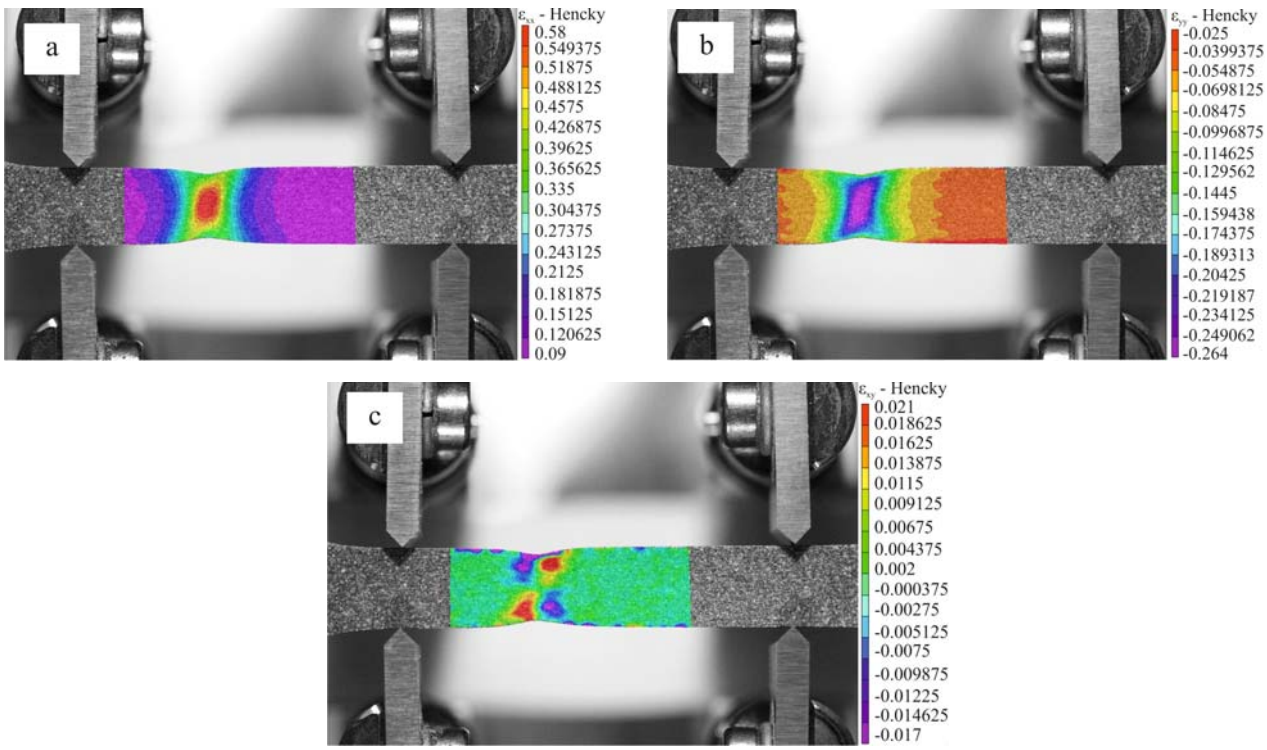

Fig. 10a,b,c. Strain fields ε_x, ε_y and γ_{xy} (–) obtained by the VIC 2D for 58 % strain.

The rod was extended with increasing force evenly throughout length after exceeding the yield strength. The permanent deformation in terms of the microstructure indeed happens quite unevenly, but at the macro level, we can consider the deformation as uniform along the entire length of the test bar. Therefore, this stage is called the region of uniform (homogeneous) deformation and is terminated at the moment of the first appearance of the local bar narrowing, which begins to form so-called neck. Therefore, the experiment results shown in this article were focused on the last stage, when the rod formed a local constriction (contraction), mainly in the width, and the rod deformed further only in this one place until it broke. In places distant from the neck, the test rod did not extend. From the results displayed in Figs. 8, 10, we can

Table 3. Material parameters obtained by the Camfit program

Specimen	E (GPa)	μ	K	ε_0	n	R_e (MPa)
1	163.4	0.292	1081.7	0.109	0.222	509.3

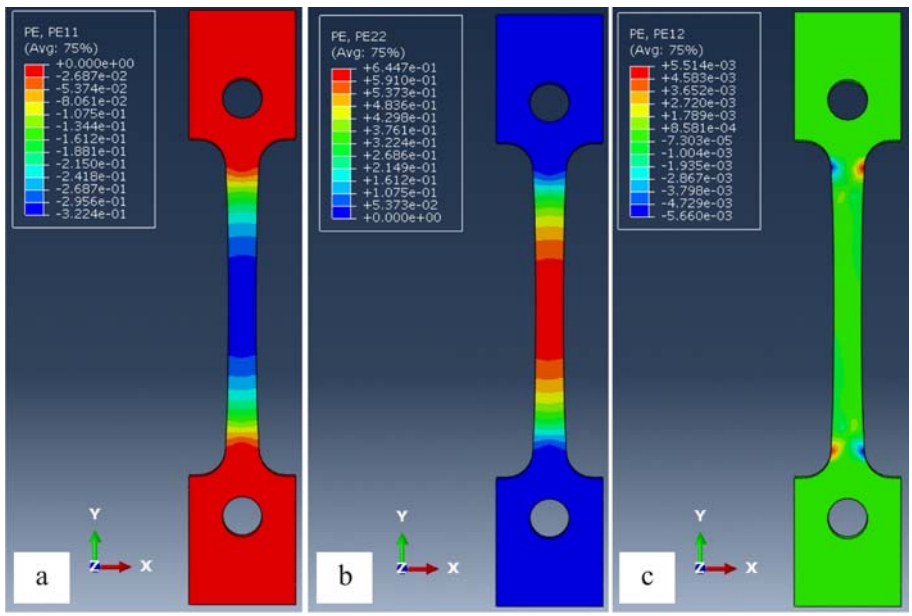

Fig. 11a,b,c. Plastic strain fields ε_x, ε_y and γ_{xy} (–) obtained by FEM.

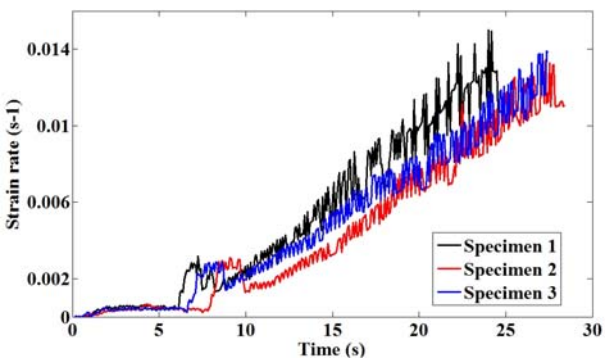

Fig. 12. The strain rate versus time diagram.

see that the maximum values of strains 25 and 58 % are shown in red in the narrowed area of the specimens. The last result of maximum strain was shown for the image, in which the added extensometer from tensile machine can still be seen. The local strain at fracture is shown in Fig. 10, after this moment the specimen was broken.

The results of strain fields obtained by finite element method exhibit approx. 20 % difference in values while the differences are in the hundredths place. The results of strain fields obtained by digital image correlation can be distorted by the facets on the edges of the specimens.

3.3. Parameters determined by virtual fields method

Displacement fields measured by digital image correlation were consequently exported to Camfit program and then the strain fields were calculated. The parameters were subsequently calculated in the selected area in the elastic and in elastic-plastic ranges, which are listed in Table 3 and were used for subsequent calculation of stress fields by the virtual fields method, which is a part of the Camfit program.

3.4. Determination of stress fields from the measured strain fields

The isotropic elastic constants and the hardening behaviour using different constitutive laws were identified by Camfit. During the calculations the hardening was described using a Swift's law:

$$\sigma_{\mathrm{eq}} = K(\varepsilon_0 + \varepsilon_{\mathrm{eq_{pl}}})^n, \tag{5}$$

where $\varepsilon_{\mathrm{eq_{pl}}}$ is the equivalent accumulated plastic strain, and K, ε_0, n are the parameters to be identified by Camfit [15–17]. Figure 13 shows stress fields σ_x, σ_y, τ_{xy} (MPa) obtained by the Matlab program for 25 % strain (Fig. 8).

Stress fields σ_x, σ_y, τ_{xy} (MPa) obtained by the

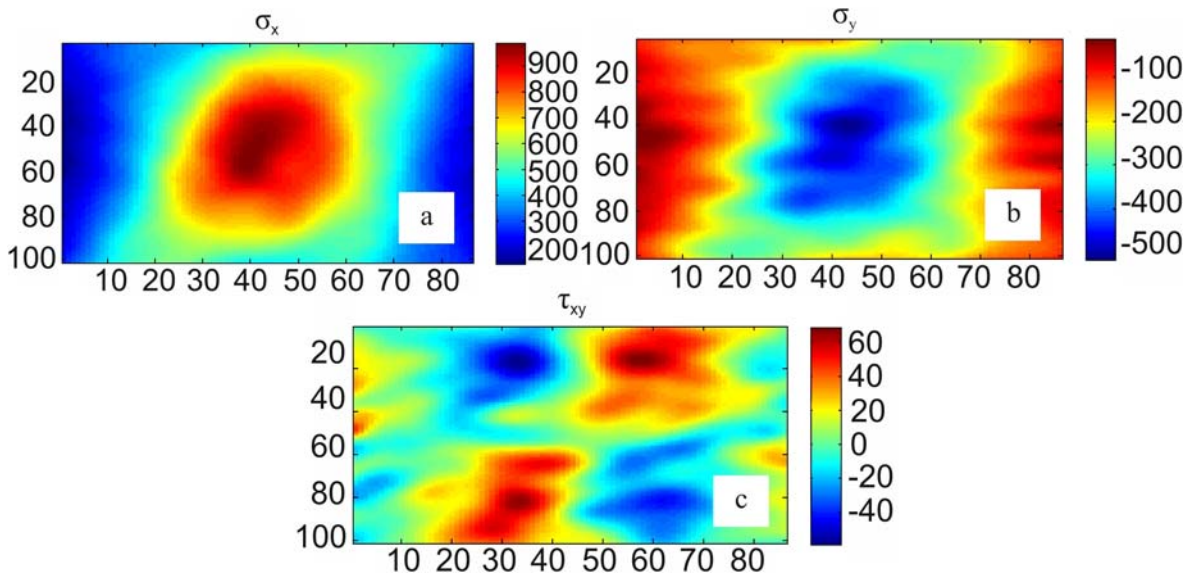

Fig. 13a,b,c. Stress fields σ_x, σ_y, τ_{xy} (MPa) obtained by the Matlab program, for 25 % strain.

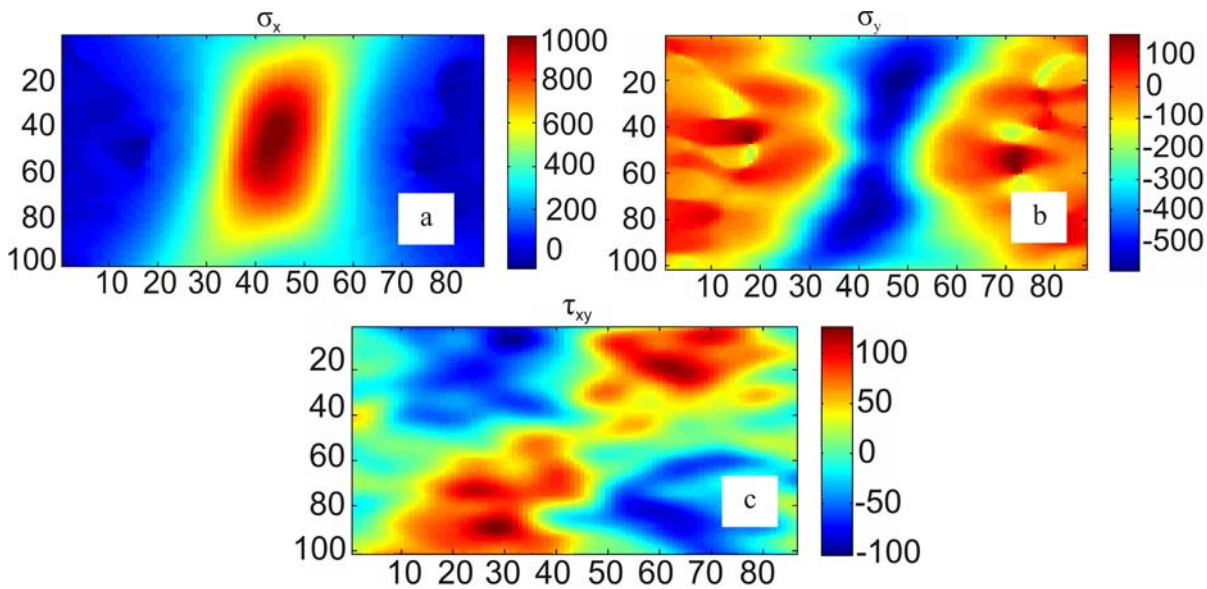

Fig. 14a,b,c. Stress fields σ_x, σ_y, τ_{xy} (MPa) obtained by the Matlab program, for 58 % strain.

Matlab program, for 58 % strain (Fig. 10) are shown in Fig. 14.

The values of true and engineering stress and their deviation for 25 and 58 % strains are listed in the Table 4.

Figure 15 shows a diagram of the true and engineering stress for the specimen 1, with marked points which correspond to the measured strain fields and calculated stress fields.

Table 4. The values of true stress and engineering stress

Specimen 1	Engineering stress (MPa)	True stress (MPa)	Deviation (%)
25 % strain	875	984	11
58 % strain	800	997	20

4. Conclusions and evaluation

The experiment was conducted on three plane specimens, made from high strength R7T steel, which is used in the manufacture of railway wheels. Since they were small, plane specimens, without an artificially created stress concentrator, the strain and stress

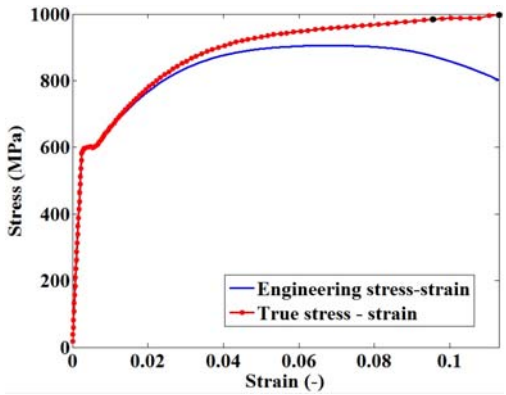

Fig. 15. Diagram of engineering and true stress for specimen 1.

at loading of the specimens were homogeneous. During the experiment the significant change beyond the yield strength occurred: when reaching approx. 8–10 % of strain, the deformation began to accumulate at the point, where subsequently a specimen narrowing (neck) occurred and it preceded the disruption of the specimen. For the reason of results consistency, the measured and calculated values are displayed only for the first specimen.

This article is aimed at evaluation of the properties of high strength steel during plastic deformation and it contains the results of the measured strain fields using the digital image correlation. Values thus obtained are shown for 25 % strain, at which the strain is significantly accumulated into the aforementioned point, and for 58 % strain, leading to disruption of the specimen. The parameters for the elastic and plastic range were then calculated from the measured strain fields, by which the stress fields were calculated in given areas. The advantage of the digital image correlation method is the possibility of rendering the true stress--strain diagram, obtained from the measured values of the specimen narrowing, and the possibility of measuring the strain fields on the specimen surface, from which we can subsequently calculate the stress fields and verify them against the values in the diagram. The maximum average values of stress obtained from true stress-true strain diagram were 990 ± 21 MPa and from engineering diagram were 897 ± 18 MPa. The deviation between maximum true and engineering average values of stress was 9 %. The deviation value of true and engineering stress shown in the diagram for 25 % strain was 11 %, and for 58 % strain was 20 %. When using only the engineering diagram, we should not be able to obtain these results and therefore, this method gives us several advantages.

Digital image correlation method shows still better use in practice, as its advantages are easy operation, accurate results, and we can use it for different types of specimen. The disadvantage consists in the fact that it requires a precise adjustment of lighting and proper surface preparation of the specimen.

It has been proved that the method of digital image correlation is suitable for the determination of the strain fields on the specimen surface, which helps us to determine the distribution of strain throughout the loading process. We also can plot the true stress--true strain diagram from these measured strain fields, which helps us not only to describe the real behaviour of materials, but it also provides us with sufficient information for potential optimization of components dimensions.

Acknowledgements

This article has been elaborated in the framework of the project Opportunity for young researchers, reg. no. CZ.1.07/2.3.00/30.0016, supported by Operational Programme Education for Competitiveness and co-financed by the European Social Fund and the state budget of the Czech Republic, and the Project No. LO1203 "Regional Materials Science and Technology Centre – Feasibility Program" funded by Ministry of Education, Youth and Sports of the Czech Republic.

References

[1] Abouridouane, M., Klocke, F., Lung, D., Adams, O.: CIRP Annals – Manufacturing Technology, *61*, 2012, p. 71. doi:10.1016/j.cirp.2012.03.075
[2] Ghadbeigi, H., Pinna, C., Celotto, S.: Experimental Mechanics, *52*, 2012, p. 1483. doi:10.1007/s11340-012-9612-6
[3] Tarantino, M. G., Beretta, S., Foletti, S., Papadopoulos, I.: International Journal of Fatigue, *46*, 2013, p. 67. doi:10.1016/j.ijfatigue.2012.05.007
[4] Wang, J., Levkovitch, V., Reusch, F., Svendsen, B., Huétink, J., Van Riel, M.: International Journal of Plasticity, *24*, 2008, p. 1039. doi:10.1016/j.ijplas.2007.08.009
[5] Purkar, T. S., Pathak, S.: ISCA J. Engineering Sci., *1*, 2012, p. 26.
[6] Sreenivasulu, R., Rao, Ch. S.: Res. J. Engineering Sci., *2*, 2013, p. 21.
[7] Holzmann, M., Jurášek, L., Dlouhý, I.: International Journal of Fracture, *148*, 2007, p. 13. doi:10.1007/s10704-007-9173-3
[8] Zaretsky, E. V.: Materials Science and Technology, *28*, 2012, p. 58. doi:10.1179/1743284711Y.0000000043
[9] Pierron, F., Grédiac, M.: The Virtual Fields Method. New York, Springer 2012. doi:10.1007/978-1-4614-1824-5
[10] Šimčák, F., Štamborská, M., Huňady, R.: Chemické Listy, *105*, 2011, p. 564.
[11] Rossi, M., Broggiato, G. B., Papalini, S.: Meccanica, *43*, 2008, p. 185. doi:10.1007/s11012-008-9123-9
[12] Sutton, M. A., Deng, X., Liu, J., Yang, L.: Experimental Mechanics, *36*, 1996, p. 99. doi:10.1007/BF02328705

[13] Sozen, S., Guler, M.: Optics and Lasers in Engineering, *49*, 2011, p. 1428. doi:10.1016/j.optlaseng.2011.07.002
[14] Sutton, M. A., Orteu, J. J., Schreier, H.: Image Correlation for Shape, Motion and Deformation Measurements. New York, Springer 2009. doi:10.1007/978-0-387-78747-3_1
[15] Rossi, M., Pierron, F., Štamborská, M., Šimčák, F.: In: Proceedings of the 2012 Annual Conference on Experimental and Applied Mechanics, Experimental and Applied Mechanics. Volume 4. Eds.: Ventura, C. E., Crone, W. C., Furlong, C. New York, Springer 2013, p. 229.
[16] Rossi, M., Pierron, F.: Comput Mech, *49*, 2012, p. 53. doi:10.1007/s00466-011-0627-0
[17] Štamborská, M., Šimčák, F., Kalina, M., Schrötter, M.: Procedia Engineering, *48*, 2012, p. 665. doi:10.1016/j.proeng.2012.09.568